Synthesis of new low band gap dyes with BF$_2$–azopyrrole complex and their use for dye-sensitized solar cells

John A. Mikroyannidis [a,*], M.S. Roy [d], G.D. Sharma [b,c,**]

[a] Chemical Technology Laboratory, Department of Chemistry, University of Patras, GR-26500 Patras, Greece
[b] Physics Department, Molecular Electronic and Optoelectronic Device Laboratory, JNV University, Jodhpur (Raj.) 342005, India
[c] Jaipur Engineering College, Kukas, Jaipur (Raj.), India
[d] Defence Laboratory, Jodhpur (Raj.), India

ABSTRACT

The diazonium salt derived from 4-aminobenzoic acid, 4-aminophenol or 2-aminophenol reacted with half equivalent of pyrrole to afford symmetrical 2,5-bisazopyrroles. They reacted subsequently with boron trifluoride in the presence of triethylamine to afford the corresponding BF$_2$–azopyrrole complexes **D1**, **D2** and **D3** respectively. They were soluble and stable in nonprotic solvents such as chloroform, dichloromethane and tetrahydrofuran but unstable in protic solvents such as ethanol. Their absorption spectra were broad with optical band gap of 1.49–1.70 eV. Among these dyes **D2** displayed the broader absorption spectrum with low band gap E_g^{opt} of 1.49 eV. We have utilized these complexes as photosensitizers for quasi solid state dye-sensitized solar cells (DSSCs) and achieved power conversion efficiency in the range of 4.0–6.0%. We have also found that the co-adsorption of citric acid hindered the formation of dye aggregates and might improve the electron injection efficiency leading to an enhancement in short circuit photocurrent. This work suggests that metal-free dyes based on BF$_2$–azopyrrole complex are promising candidates for improvement of the DSSC performance.

© 2010 Elsevier B.V. All rights reserved.

1. Introduction

Dye-sensitized solar cells (DSSCs) based on dye sensitizers adsorbed on nanocrystalline TiO$_2$ electrodes have received considerable attention because of their high incident solar light-to-electricity conversion efficiency, colourful and decorative natures and low cost of production [1], since O'Regan and Grätzel reported good solar cell performances for DSSCs based on a Ru complex dye in 1991 [2]. Along with Ru-sensitizers, metal-free organic dyes have recently been stimulating intensive research efforts because of their advantages as photosensitizers for DSSCs: (1) they can be prepared and purified easily at low cost, (2) they have higher molar absorption coefficients than the Ru complexes, which indicates that they have efficient light-harvesting capabilities over the wide spectral region of sunlight, (3) the wide variety of the structures and their facile modification provides potential for molecular design, with the introduction of substituents onto the chromophore skeletons allowing easier control not only of their photophysical and

electrochemical properties but also of their stereochemical structures as well, and finally (4) there are no concerns about resource limitations, because organic dyes do not contain rare metals such as ruthenium and platinum. Many organic dyes exhibiting relatively high DSSC performances have so far been designed and developed [1]. They include dyes derived from coumarin, polyene, hemicyanine, thiophene, indoline, heteropolycyclic, xanthene, perylene, porphyrin, merocyanine, catechol, squaraine, cyanine and phthalocyanine. Under standard air mass (AM) 1.5 simulated sunlight (100 mW cm^{-2}), the DSSC based on indoline dye D205 has shown a power conversion efficiency (PCE) of up to 9.5%, with a short circuit photocurrent density (J_{sc}) of 18.7 mA cm^{-2}, an open circuit photovoltage (V_{oc}) of 710 mV and a fill factor (FF) of 0.71. The incident photon to current conversion efficiency (IPCE) in the visible is over 80%. The performances of organic dye-based DSSCs remain inferior to those of DSSCs based on the Ru complexes, however, because of some disadvantages that they exhibit as photosensitizers: (1) they have relatively narrow absorption bands in the visible, which cause poorer light-harvesting in sunlight, (2) they are liable to enter into π-stacked aggregation on the TiO$_2$ surface, which leads to reductions in the yields of electron injection from the dyes to the conduction band (CB) of TiO$_2$, owing to intermolecular energy transfer, and (3) the stabilities of organic dyes are generally lower than those of Ru complexes, which may be attributable to the formation of unstable radicals under strong light irradiation

* Corresponding author. Tel.: +30 2610 997115; fax: +30 2610 997118.
** Corresponding author at: Jaipur Engineering College, Kukas, Jaipur (Raj.), India.
Tel.: +91 0291 2720857; fax: +91 0291 2720856.
E-mail addresses: mikroyan@chemistry.upatras.gr (J.A. Mikroyannidis), sharmagd_in@yahoo.com (G.D. Sharma).

[1]. Therefore, to overcome the above disadvantages as photosensitizers for DSSCs, it is necessary to design and synthesize new and efficient organic photosensitizers with effective chromophores and substituents for the performance of DSSCs, to be made possible by exquisite molecular designs and synthetic strategies developed by organic chemists.

One of the limiting parameters in plastic solar cells is the mismatch of their absorption to the terrestrial solar spectrum. The use of low band gap materials ($E_g < 1.8\,eV$) is a viable route to enhance the number of photons absorbed. To construct polymers consisting of alternating electron-rich and electron-deficient aromatic units is the most successful strategy to lower the optical band gap of the conjugated polymers [3]. Various electron-deficient units, e.g., electron-deficient heterocycles [4,5], perylene diimides [6], cyanovinylenes [7], and several electron-rich units, e.g., thiophene, pyrrole, fluorene and carbazole, have been used to construct low band gap materials. Diketopyrrolopyrrole (DPP) derivatives, with the pyrrolo[3,4-c]pyrrole-1,4-dione unit as the underlying chromophore system, have been extensively studied for bulk heterojunction (BHJ) solar cells [8–10]. On the other hand, dithieno[3,2-b:2′,3′-d]pyrrole (DTP) has good planarity and stronger electron-donating ability of nitrogen atoms, properties that may lead to the development of a low band gap polymer when it is copolymerized with an acceptor such as dithienylbenzothiadiazole. Several publications have reported its use for BHJ solar cells [11,12].

Azo compounds belong to one of the most intensively studied groups for non-linear optics (NLO) [13–15], optical information storage [16], and optical switching [17]. Besides their classical applications in synthetic dyes and pigments, they find increasing accessibility in photoresponsive biomaterials and supramolecular systems. They combine their optical and electronic properties with good chemical stability and solution processability [18,19], which makes them interesting for applications. Thiaxole-containing azo compounds were synthesized and their photovoltaic (PV) properties investigated using a sandwich cell with Al and Ag electrodes [20].

Very recently, a series of symmetrical 2,5-bisazopyrroles were synthesized by a one-step reaction of substituted phenyl diazonium salts with pyrrole under basic conditions [21]. The reaction of 2,5-bis(4-dimethylaminophenylazo)-pyrrole with boron trifluoride provided a BF_2–azopyrrole complex with near-infrared absorption spectrum. Based on this investigation we synthesized three new bisazopyrrole dyes and the corresponding BF_2–azopyrrole complexes. These symmetrical dyes contain carboxy or hydroxy anchoring groups at both sides of their molecules. They were conveniently synthesized by a two-step reaction sequence starting from widely available and inexpensive starting materials. Bisazopyrroles exhibit broad absorption spectra which are further shifted bathochromically by complexation with BF_3 [21].

So far there are few reports on DSSCs with pyrrole as sensitizers [22]. Therefore, we have synthesized the pyrrole-based dyes and evaluate their potential as sensitizer for DSSCs. A series of azopyrrole-based dyes have been synthesized and DSSCs using these materials as sensitizer have been discussed in detail.

2. Experimental

2.1. Characterization methods

IR spectra were recorded on a Perkin-Elmer 16PC FT-IR spectrometer with KBr pellets. ^1H NMR (400 MHz) spectra were obtained using a Brucker spectrometer. Chemical shifts (δ values) are given in parts per million with tetramethylsilane as an internal standard. UV–vis spectra were recorded on a Beckman DU-640

spectrometer with spectrograde THF. Elemental analyses were carried out with a Carlo Erba model EA1108 analyzer.

2.2. Reagents and solvents

Tetrahydrofuran (THF) was dried by distillation over CaH_2. Triethylamine was purified by distillation over KOH. 4-Aminobenzoic acid was recrystallized from water. 4-Aminophenol was purified by sublimation at $110\,°C/0.3\,mm$. 2-Aminophenol was purified by dissolution in hot water, decolourized with activated charcoal, filtered and cooled to induce crystallization. All other reagents and solvents were commercially purchased and were used as supplied.

2.3. Synthesis of bisazopyrroles

2.3.1. 2,5-Bis(4-carboxyphenylazo)-1H-pyrrole (*2a*)

A flask was charged with a suspension of 4-aminobenzoic acid (1.10 g, 8.00 mmol) in water (10 mL). Hydrochloric acid (2 mL) was added to the suspension until the mixture was homogenous. The solution was cooled and kept at $0–5\,°C$ in an ice bath and diazotized by addition of a solution of $NaNO_2$ (0.56 g, 8.11 mmol) in water (5 mL) followed by stirring for 0.5 h at $0–5\,°C$. The solution of 4-carboxyphynyl diazonium salt (*1a*) thus prepared was immediately used for the next coupling reaction.

The solution of 4-carboxyphynyl diazonium salt (*1a*) was slowly added to a solution of pyrrole (0.27 g, 4.02 mmol) and pyridine (2 mL) in methanol (30 mL) at $0–5\,°C$. The resulting mixture was stirred for 10 h and then concentrated under reduced pressure. The precipitate was filtered, washed with water and dried to afford *2a*. It was purified by column chromatography, eluting with a mixture of dichloromethane and hexane (1:1). Yield 80% (1.16 g).

FT-IR (KBr, cm^{-1}): 3404 (N–H stretching); 2994 (O–H stretching); 1686 (carbonyl); 1600, 1420 (aromatic); 1164, 770 (pyrrole ring).

^1H NMR (CDCl$_3$) ppm: 12.10 (Br, 2H, carboxyl); 9.80 (s, 1H, NH of pyrrole); 8.13 (m, 4H, aromatic ortho to carboxyl); 7.80 (m, 4H, aromatic ortho to azo); 6.85 (s, 2H, aromatic of pyrrole).

Anal. Calcd. for C$_{18}$H$_{13}$N$_5$O$_4$: C, 59.50; H, 3.61; N, 19.28. Found: C, 58.96; H, 3.47; N, 19.14.

2.3.2. 2,5-Bis(4-hydroxyphenylazo)-1H-pyrrole (*2b*)

Starting from 4-aminophenol compound *2b* was similarly synthesized in 75% yield.

FT-IR (KBr, cm^{-1}): 3407 (N–H stretching); 3120 (O–H stretching); 1216, 1174 (C–OH stretching); 1356, 1330 (O–H deformation); 1598, 1500, 1438 (aromatic); 1154, 746 (pyrrole ring).

^1H NMR (CDCl$_3$) ppm: 9.78 (s, 1H, NH of pyrrole); 7.70 (m, 4H, aromatic ortho to azo); 6.84 (m, 4H, aromatic ortho to hydroxyl, and 2H, aromatic of pyrrole); 5.35 (s, 2H, hydroxyl).

Anal. Calcd. for C$_{16}$H$_{13}$N$_5$O$_2$: C, 62.53; H, 4.26; N, 22.79. Found: C, 62.15; H, 4.37; N, 22.48.

2.3.3. 2,5-Bis(2-hydroxyphenylazo)-1H-pyrrole (*2c*)

Starting from 2-aminophenol compound *2c* was similarly synthesized in 73% yield.

FT-IR (KBr, cm^{-1}): 3410 (N–H stretching); 3114 (O–H stretching); 1222, 1196 (C–OH stretching); 1382, 1342 (O–H deformation); 1586, 1508, 1448 (aromatic); 1158, 750 (pyrrole ring).

^1H NMR (CDCl$_3$) ppm: 9.79 (s, 1H, NH of pyrrole); 7.80 (d, 2H, aromatic ortho to azo); 7.24 (m, 2H, aromatic meta to hydroxyl); 6.93 (m, 2H, aromatic para to hydroxyl); 6.85 (m, 2H, aromatic ortho to hydroxyl, and 2H, aromatic of pyrrole); 5.37 (s, 2H, hydroxyl).

Anal. Calcd. for C$_{16}$H$_{13}$N$_5$O$_2$: C, 62.53; H, 4.26; N, 22.79. Found: C, 61.96; H, 4.13; N, 22.12.

2.4. Synthesis of BF_2–azopyrrole complexes

2.4.1. 2,5-Bis(4-carboxyphenylazo)pyrrole-1-boron difluoride (**D1**)

To a solution of **2a** (0.20 g) and triethylamine (2 mL) in dry chloroform (20 mL) was slowly added boron trifluoride diethyl etherate (1 mL) under N_2. The resulting solution was refluxed for 2 h and then evaporated to dryness. The residue was triturated with ether, filtered and dried to afford the triethylammonium salt of **D1** as a dark purple product (0.26 g, 76%).

FT-IR (film on NaCl cell, cm^{-1}): 2988 (C–H stretching of triethylamine); 1692 (carbonyl); 1602, 1470 (aromatic); 1062 (BF_2–azopyrrole complex).

^{1}H NMR ($CDCl_3$) ppm: 8.12 (m, 4H, aromatic ortho to carboxyl); 7.88 (m, 4H, aromatic ortho to azo); 6.94 (s, 2H, aromatic of pyrrole); 2.62 (m, 12 H, NCH_2CH_3); 1.33 (t, 18H, NCH_2CH_3). The carboxylic proton was unobserved.

Anal. Calcd. for $C_{30}H_{42}BF_2N_7O_4$: C, 58.73; H, 6.90; N, 15.98. Found: C, 57.93; H, 6.74; N, 16.10.

2.4.2. 2,5-Bis(4-hydroxyphenylazo)pyrrole-1-boron difluoride (**D2**)

Starting from **2b** compound **D2** was similarly synthesized in 81% yield.

FT-IR (film on NaCl cell, cm^{-1}): 3174 (O–H stretching); 1180 (C–OH stretching); 1394 (O–H deformation); 1609, 1502, 1426 (aromatic); 1066 (BF_2–azopyrrole complex).

^{1}H NMR ($CDCl_3$) ppm: 7.90 (m, 4H, aromatic ortho to azo); 6.94–6.84 (m, 4H, aromatic ortho to hydroxyl, and 2H, aromatic of pyrrole); 5.34 (s, 2H, hydroxyl).

Anal. Calcd. for $C_{16}H_{12}BF_2N_5O_2$: C, 54.12; H, 3.41; N, 19.72. Found: C, 53.79; H, 3.56; N, 19.48.

2.4.3. 2,5-Bis(2-hydroxyphenylazo)pyrrole-1-boron difluoride (**D3**)

Starting from **2c** compound **D3** was similarly synthesized in 78% yield.

FT-IR (film on NaCl cell, cm^{-1}): 3156 (O–H stretching); 1180 (C–OH stretching); 1396 (O–H deformation); 1606, 1484, 1470 (aromatic); 1074 (BF_2–azopyrrole complex).

^{1}H NMR ($CDCl_3$) ppm: 7.85 (d, 2H, aromatic ortho to azo); 7.26 (m, 2H, aromatic meta to hydroxyl); 6.92 (m, 2H, aromatic para to hydroxyl); 6.85 (m, 2H, aromatic ortho to hydroxyl, and 2H, aromatic of pyrrole); 5.35 (s, 2H, hydroxyl).

Anal. Calcd. for $C_{16}H_{12}BF_2N_5O_2$: C, 54.12; H, 3.41; N, 19.72. Found: C, 53.86; H, 3.28; N, 19.54.

2.5. Electrochemical measurements

The cyclic voltammetry measurements were performed on an Autolab Potentiostat PGSTAT-10 in acetonitrile solution (0.1 M) of 4-*tert*-butylpyridine (TBP) at a potential sweep of $0.05 V s^{-1}$ at room temperature. A glassy carbon electrode coated with a thin film of the pyrrole dye was used as working electrode. Pt and Ag wires were used as working electrode and reference electrode, respectively. The electrochemical potential was calibrated against Ag/AgCl.

2.6. Assembly and characterization of DSSCs

The average size of commercial P25 TiO_2 particle is about 25 nm and has a mix crystal structure which consists of 30% rutile and 70% anatase. The paste of TiO_2 was prepared as follows: 12 g TiO_2 power was ground in a porcelain mortar with 4 mL ethanol containing 0.4 mL accetylacetone to prevent re-aggregation of the particles, and then it was diluted by slow addition of water under continuous grinding. Finally, a detergent (0.2 mL Triton X-100) was added and a viscous paste of TiO_2 nanoparticles was obtained. The FTO (fluorine doped SnO_2) glass, sheet resistance 10–15 Ω sq^{-1}, transmission >90% in visible light) was first cleaned in a detergent solution using an ultrasonic bath for 15 min, and then rinsed with water and ethanol. The washed FTO glass was immerged in 40 mL aqueous $TiCl_4$ solution at 70 °C for 30 min and then washed with water and ethanol. The prepared TiO_2 paste was deposited on the $TiCl_4$ treated FTO glass substrate by the doctor blade method, i.e. spreading the paste by sliding a glass rod on the side of FTO glass. The TiO_2-coated FTO glass was sintered at 450 °C for 30 min in air atmosphere. This post-treatment results in enhancement in PCE of DSSCs due to the improved inter-particle bridge in the TiO_2 film [23,24]. After the film was cooled to 60 °C, it was immersed in 5×10^{-4} M dye solution in THF and maintained under dark conditions for overnight. Quasi solid state polymer electrolyte was prepared by adding 0.083 g of P25 TiO_2 powder, 0.1 g of LiI, 0.019 g of I_2, and 0.264 g of PEO, 1:1 accetone/propylene carbonate solution. Finally, the electrolyte was spin coated over the dye-sensitized TiO_2 electrode. To prepare the platinum counter electrode, H_2PtCl_6 solution in iso-propanol (2 mg mL^{-1}) was deposited onto the FTO glass substrates and then was sintered at 400 °C for 30 min. The DSSCs were fabricated by sandwiching the electrolyte between the dye-sensitized photoanode and the counter electrode and assembly was held together using mini-binder clips.

2.7. Photovoltaic measurements

The current–voltage (J–V) characteristics in dark and under illumination were obtained by a Keithley electrometer with built in power supply. A 100W halogen lamp was used as light source and the intensity of the light is about 100 mW cm^{-2} measured with the lux meter equipped with silicon detector. The electrochemical impedance spectra (EIS) measurements were carried out by applying bias of the open circuit voltage (V_{oc}) and recorded over a frequency range of 1 mHz–10^5 Hz with ac amplitude of 10 mV. The above measurements were recorded with an Autolab Potentiostat PGSTAT-10 equipped with frequency response analyzer (FRA).

3. Results and discussion

3.1. Synthesis and characterization

Scheme 1 outlines the synthesis of the three bisazopyrrole dyes and the corresponding BF_2–azopyrrole complexes. Specifically, 4-aminobenzoic acid, 4-aminophenol or 2-aminophenol reacted with sodium nitrite/aqueous HCl at temperature 0–5 °C to afford the substituted phenyldiazonium salts **1a**, **1b** and **1c**. The latter reacted subsequently with half equivalent of pyrrole in methanol neutralized with pyridine to give the symmetrical bisazopyrroles **2a**, **2b** and **2c**. Finally, they reacted with boron trifluoride etherate in the presence of triethylamine to form the corresponding BF_2–azopyrrole complexes **D1**, **D2** and **D3** [21]. These complexes were soluble and stable in nonprotic solvents like THF, dichloromethane, chloroform, acetonitrile etc., but unstable in protic solvents like ethanol [21]. **D1** was obtained as triethylammonium salt.

The complexation of bisazopyrroles with boron trifluoride aimed to shift bathochromically their absorption spectrum. Apparently, this results from significant π-electron delocalization in the planar structure dominated by complexation of the electron-withdrawing BF_2 group [21]. During the complexation the colour of the reaction solution changed from red to dark purple. Clear evidence for the complexation was obtained from the FT-IR spectra of **D1**, **D2** and **D3**. They, as compared to the corresponding parent bisazopyrroles, showed a new intense absorption band around 1070 cm^{-1} assigned to the BF_2–azopyrrole complex.
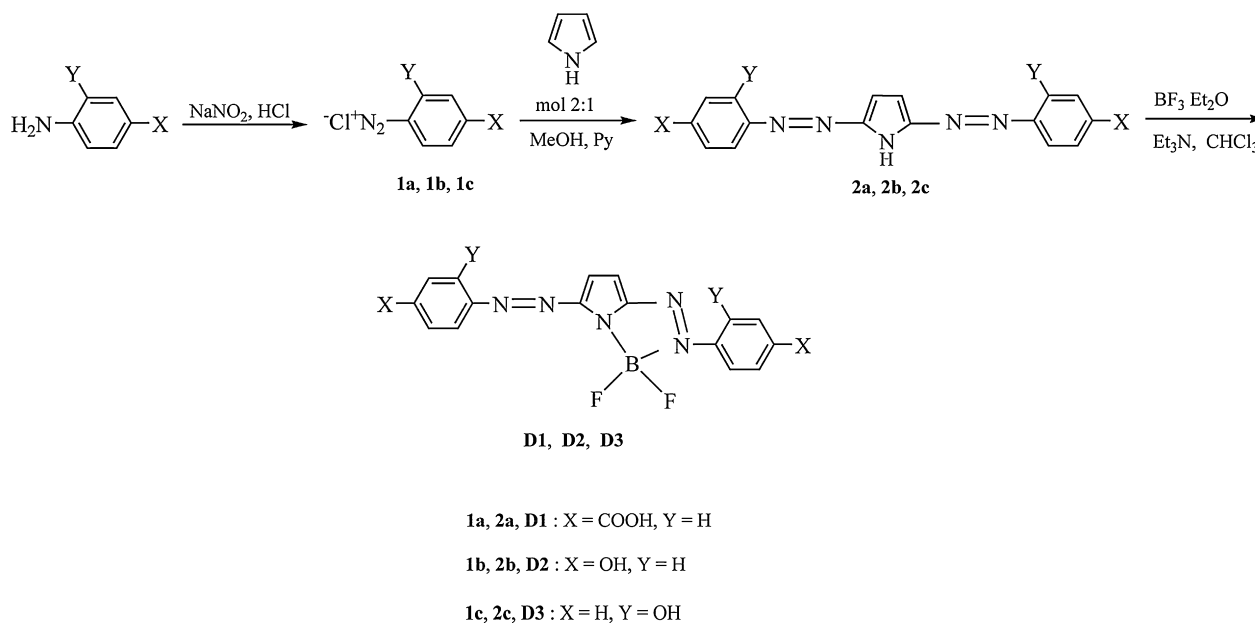
Scheme 1. Synthesis of bisazopyrroles and BF_2–azopyrrole complexes.

3.2. Photophysical and electrochemical properties

Fig. 1 presents the UV–vis absorption spectra of **D1**, **D2** and **D3** in dilute (10^{-5} M) THF solution and thin film. Their photophysical characteristics are summarized in Table 1. The absorption
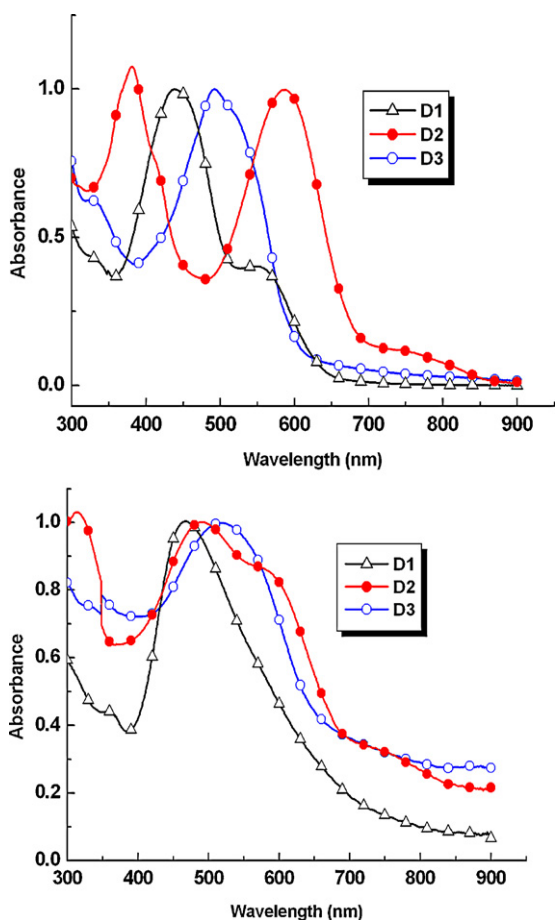
Fig. 1. UV–vis spectra of **D1**, **D2** and **D3** in THF solution (top) and thin film (bottom).

spectra of these BF_2–azopyrrole complexes showed a broad absorption band covering the visible and near-infrared region. For the dye films the absorption bands were broader than their solutions, which can be attributed to the inter-chain interactions in solid state. The absorption maxima ($\lambda_{a,max}$) of the dyes are located at the range of 328–586 nm (Table 1). The short-wavelength maxima ($\lambda_{\alpha,max}$ < 400 nm) correspond to the π–π^* absorption of the molecules, while the long-wavelength maxima ($\lambda_{\alpha,max}$ > 400 nm) could be assigned to the intramolecular charge transfer transition between the BF_2–azopyrrole central unit and the terminal carboxy- or hydroxy-substituted phenyls. The near-infrared absorption of the BF_2–azopyrrole complexes is dominated by π-resonance effects, which was achieved by extending conjugation around N=N bond and forming rigid azo configuration. Thus the reaction of bisazopyrroles **2a**, **2b** and **2c** with BF_3 Et$_2$O that results in their complexation provides an effective and simple method to synthesize such dyes by enhancing π-electron delocalization.

Upon comparing the absorption spectra of the complexes, **D2** showed the broader spectrum which was extended up to ~850 nm both in solution and thin film. Specifically, **D2** displayed a shoulder around 750 nm which widen its absorption band. The thin film absorption onset of **D1**, **D2** and **D3** was found to be at 732, 835 and 805 nm which corresponds to an optical band gap (E_g^{opt}) of 1.70, 1.49 and 1.54 eV respectively (Table 1). An alternating phenylenevinylene copolymer with 2,5-bisazopyrrole segments along the backbone was synthesized in our laboratory very recently

Table 1
Optical and electrochemical properties of dyes **D1**, **D2** and **D3**.

Sample	D1	D2	D3
$\lambda_{a,max}$[a] in solution (nm)	439, 551	381, 586	328, 491
$\lambda_{a,max}$[a] in thin film (nm)	468	489, 581	518
Thin film absorption onset (nm)	732	835	805
E_g^{opt}[b] (eV)	1.70	1.49	1.54
HOMO (V/ vs NHE)	0.76	0.80	0.86
LUMO (V/vs NHE)	−0.98	−0.74	−0.72
E_g^{el} (eV)[c]	1.74	1.54	1.58

[a] $\lambda_{a,max}$: the absorption maxima from the UV–vis spectra in THF solution or in thin film.
[b] E_g^{opt}: optical band gap determined from the absorption onset in thin film.
[c] E_g^{el}: Electrochemical band gap determined from cyclic voltammetry.
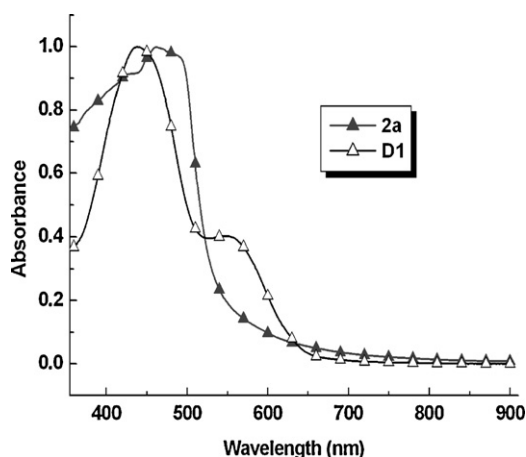
Fig. 2. UV–vis spectra of **D1** and **2a** in THF solution.

[25]. The BF$_2$–azopyrrole complex of this copolymer exhibited E_g^{opt} value of 1.63 eV.

Fig. 2 presents the UV–vis absorption spectra in THF solution of dye **D1** and the intermediate 2,5–bisazopyrrole **2a** for comparison. As it can be seen from this figure, the curve of **D1** was broader than that of the **2a**. In particular, **D1** displayed a shoulder approximately at 550 nm which broadened the absorption curve. Thus, the absorption onset was located at 640 nm for **D1** and 535 nm for **2a**. This supports the superiority of **D1** against **2a** with respect their absorption and consequently their photovoltaic properties. Dyes **D2** and **D3** were similarly superior to **2b** and **2c**, respectively.

The normalized absorption spectra of the pyrrole dyes adsorbed onto the TiO$_2$ films were shown in Fig. 3. Compared with the absorption spectrum in solution, the absorption spectrum of the dyes attached to TiO$_2$ film were broaden significantly and nearly a 50 nm redshifted of the maxima absorption peak was observed, which can be attributed to the formation of a J-type aggregate. Similar J-type aggregation has been reported using deketopyrrole dyes [26]. It is clearly seen that the absorption spectra of all dyes adsorbed on TiO$_2$ films were broadened in comparison with those in solution due to the interaction of anchoring group with the surface of titanium ions [27]. The redshift in the absorption spectra of dye absorbed TiO$_2$ film is attributed to the increased delocalization of the π^* orbital of dye caused by the interaction between the anchoring group present in the dye and the Ti^{4+} ions, which directly decreases the energy of the π^* level. The amounts of the adsorbed dye on the TiO$_2$ films were estimated by desorbing the dye in basic solution. The surface concentration was determined to be 2.04×10^{-7}, 2.67×10^{-7} and 3.14×10^{-7} mol cm^{-2}, for **D3**, **D2** and **D1** dyes, respectively.
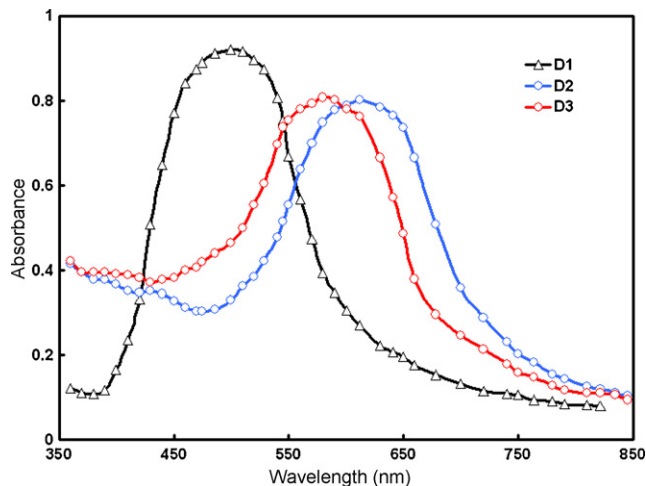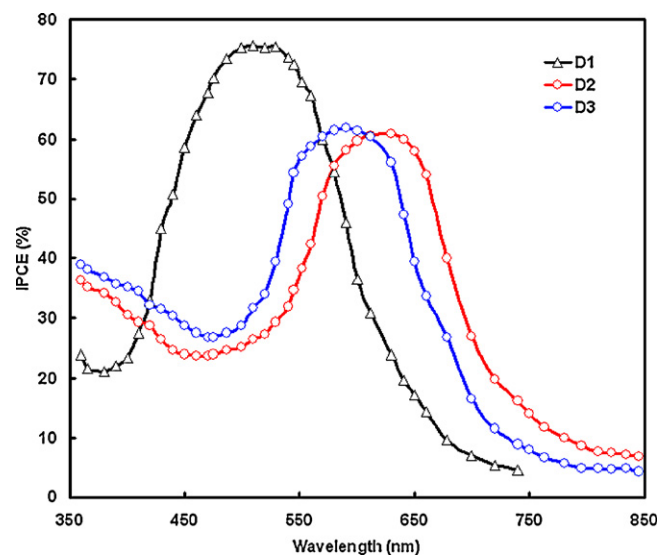
The position of the HOMO and LUMO of the organic material used for sensitizer in DSSCs also affects their PV performance. To investigate the possibilities of the electron transfer from the excited state (LUMO) of the dye molecules, into the conduction band of the TiO$_2$ nanocrystalline film and the dye regeneration, the oxidation and reduction potentials were measured via cyclic voltammetry (CV) measurements. The HOMO and LUMO energy levels of the dyes are estimated from the onset oxidation and reduction potential observed in the CV using the following expression:

$$E_{LUMO} = -(E_{red}^{onset} + 4.70)\,eV$$
$$E_{HOMO} = -(E_{ox}^{onset} + 4.70)\,eV$$

The electrochemical parameters of the three pyrrole dyes are summarized in Table 1. It can be seen from this table that the positions of the oxidation potential and reduction potential of all three dyes agreed well with the requirement for an efficient sensitizer. On one hand, the oxidation potentials of all three dyes are more positive than the iodine redox potential (0.42 V) [28]. An oxidation potential higher than that of redox potential of iodine couple is necessary to reduce the backward electron transfer to electrolyte solution in DSSCs. Moreover, the oxidation potential (HOMO level) of the sensitizer dyes is more positive than the iodine/iodide redox potential, which indicates that there is enough driving force for the efficient dye regeneration through the recapture injected electrons from I$^-$ by the dye cation radical. On the other hand, the reduction potential for all dyes is more negative than the equivalent potential for TiO$_2$ conduction band (-0.5 V vs NHE). It can be seen from Table 1 that the energy gap between the onset reduction potential (LUMO) and the equivalent potential for TiO$_2$ conduction band is in the range 0.2–0.45 V. This difference is higher than 0.2 V, which is necessary for the efficient electron injection from the LUMO of the sensitizer into the conduction band of TiO$_2$ [29]. As shown in Table 1, the HOMO value of **D2** and **D3** are significantly higher than that for **D1**, which could be ascribed to the better electron transfer character of the hydroxyl phenylazo units.

3.3. Photovoltaic performance of DSSCs

Fig. 4 shows the photoaction spectra of incident photon to current conversion efficiency (IPCE) for DSSCs based on different

Fig. 4. IPCE action spectra of the DSSCs with **D1**, **D2** and **D3** as photosensitizers.

Fig. 3. Absorption spectra of **D1**, **D2** and **D3** pyrrole dyes adsorbed on TiO$_2$ films.
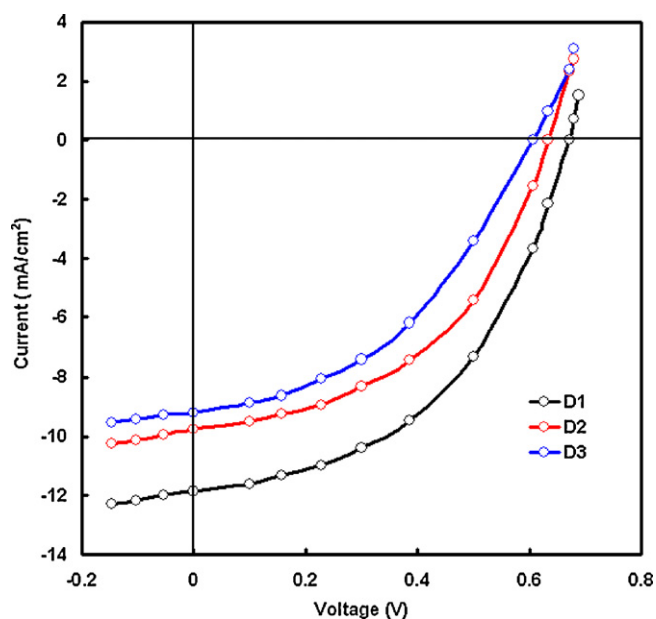
Fig. 5. Current–voltage characteristics under illumination for DSSCs based on **D1**, **D2** and **D3** pyrrole dyes.

Fig. 6. Absorption spectra of the **D1** dye-sensitized TiO_2 film with and without citric acid coadsorbent.

pyrrole dyes. The IPCE spectra of the DSSCs are consistent with the absorption spectra of the respective dye adsorbed on the TiO_2 film. The IPCE for DSSC based on **D1** sensitizer exhibits an elevated efficiency of higher than 55% in the range of 450–550 nm with maximum value of 75% around 520 nm. On the other hand, the IPCE value of DSSCs based on **D2** and **D3** is low in this particular range, suggesting poor electron injection efficiency from the LUMO of the **D2** and **D2** into the conduction band of TiO_2. The maximum IPCE value of DSSCs based on **D2** and **D3** is lower than that for DSSCs based on **D1**, in the lower wavelength region, while in the longer wavelength region the DSSCs based on **D2** and **D3** show higher IPCE. Here we would like to mention that due to the extending conjugation around N=N bond and formation of rigid azo configuration, the IPCE spectra of the DSSCs based on **D2** and **D2** extended, even to near-infrared region (>800 nm).

The PV performance of DSSCs was measured at $100\,mW\,cm^{-2}$ without using solar simulator (Fig. 5) and the PV parameters are summarized in Table 2. The low PCE of the DSSCs based on the **D2** and **D3** as compared to **D1** is due to their lower extinction coefficient (when measured on adsorbed on TiO_2 film), photocurrent and IPCE values in lower wavelength region. As the reduction potential (LUMO level) of **D1** is $-0.98\,V$ vs NHE (Table 1), is more negative than that of **D2** ($-0.74\,V$ vs NHE) and **D3** ($0.72\,V$ vs NHE), it indicates that the driving force for the injection of electrons from excited state of **D1** is higher than that for **D2** and **D3**. Therefore, the electron injection efficiency for the DSSCs based on **D1** is higher than that for **D2**- and **D3**-based DSSCs, and results an enhancement in the IPCE values and PCE in former case. Since the **D1** has COOH group for the anchoring the TiO_2 surface and **D2** and **D2** have OH group as anchoring group, the **D1** is more attached to TiO_2 surface as compared to **D2** and **D3**. Evidence for this can also be obtained from the
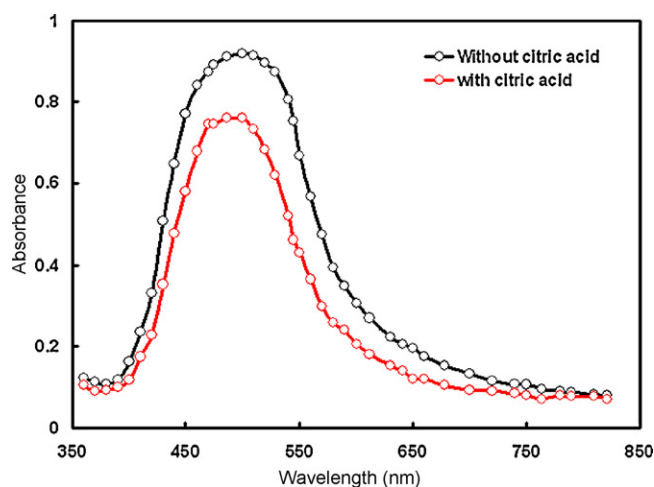
absorption spectra of the dyes on TiO_2. In particular, the absorption coefficient of **D1** on TiO_2 film is higher than that for **D2** and **D3** (Fig. 3). The higher amount of dye loading increases the light-harvesting property of the photoelectrode also which is attributed to the higher short circuit photocurrent and IPCE.

The sensitizer performances are strongly affected by some key factors which govern the efficiency of the electron injection into TiO_2 conduction band [30], such as excited state redox potential, the unidirectional electron flow from the donor moiety to the anchoring acceptor group, enhanced by the conjugation across the linker, and the electron coupling between LUMO of sensitizer and conduction band of TiO_2. Moreover, other factors that play a prominent role in determining the PCE are the charge recombination of the injected electron with the dye or oxidized electrolyte and the formation of dye aggregation on the TiO_2 surface [31]. Therefore, research strategies used to increase the PCE of DSSCs have also been focused on the use of coadsorbents [32]. Regarding this strategy, several kinds of additives such as deoxycholic acid [33], hexadecylimalonic acid [34], guanidinium thiocyanante [35] and *tert*-butylpyridine [36] have been added to DSSCs in order to improve the J_{sc} or the V_{oc} or both of the solar cells. We have used critic acid as coadsorbent and its effect on the PV performance of the DSSCs based on **D1** dye as sensitizer.

Citric acid is a tri-protic weak organic acid with three carboxylic groups on its molecular structure. The presence of these carboxylic groups ensures anchoring of this acid onto the TiO_2 surface, and it can act as a buffer on the surface of the semiconductor nanoparticles. The UV–vis absorption spectra of the **D1** dye-sensitized TiO_2 film were measured (Fig. 6). The film was immersed into a solution of **D1** dye containing 1.5 mM of citric acid. As can be seen from this figure, when TiO_2 film was immersed into the **D1** solution containing citric acid, the dye adsorption was reduced. The decrease in the dye adsorption indicates that citric acid competes for the TiO_2 surface sites with the dye molecules. Strong interaction between the adsorbed dye molecules and the oxide molecules in the TiO_2 leads to aggregate formation and consequently, broadening of absorp-

Table 2
Photovoltaic parameters of DSSCs based on different pyrrole dyes as sensitizers.

Dye	Short circuit current (J_{sc}) (mA cm^{-2})	Open circuit voltage (V_{oc}) (V)	Fill factor (FF)	Power conversion efficiency (η) (%)
D1	11.85	0.68	0.64	5.15
D1 with coadsorbent	12.50	0.71	0.67	5.96
D2	9.75	0.63	0.58	3.56
D2 with coadsorbent	10.48	0.67	0.60	4.21
D3	9.2	0.61	0.54	3.03

tion spectrum, which was observed during the dye absorption. This can be related to the dye–TiO$_2$ interactions, dye–dye interaction, or both, but the co-adsorption of citric acid diminished these interactions on the TiO$_2$ surface [37]. The absorption peak showed smaller red shifts when the dye co-adsorbed with citric acid compared with the spectrum of only dye adsorbed on to the TiO$_2$ film. This indicates that the aggregation of dye molecules on the TiO$_2$ has been retarded by the co-adsorption of citric acid with dye.

The *J–V* characteristics for the DSSCs with coadsorbent are shown in Fig. 7 and the PV parameters are summarized in Table 2. It is interesting to note that the citric acid co-adsorption increases both V_{oc} and J_{sc}, resulting in the overall PCE of the DSSCs. The amount of dye loading is reduced by the addition of coadsorbent which indicates that the amount of dye is replaced by the coadsorbent on the TiO$_2$ surface. Even though the decrease in the amount of the dye loading, the J_{sc} has been improved for the DSSCs based on coadsorbent, indicating that reduction in light-harvesting by the dye due to the surface dilution with coadsorbent has been compensated by the higher electron collection efficiency due to the slower recombination rate and/or enhanced electron transport across the nanocrystalline TiO$_2$ film [38].

The coadsorbent suppresses the aggregation of the dye on the surface of the TiO$_2$, resulting in an improvement in the PCE of the DSSCs. This can be explained from the electrochemical impedance spectroscopy (EIS) of the DSSCs. EIS has proven to be a useful technique for the characteristics of electronic and ionic processes in DSSCs [39]. Generally, three characteristics peaks can be obtained from the EIS spectra (Bode phase plot), when the EIS spectra of DSSCs is measured under open circuit conditions. The low frequency peak (in mHz range) is attributed mainly to the Nernst diffusion of I$_3^-$ within the electrolyte. The middle frequency peak (in the 1–100 Hz range) is related to the transport process of the
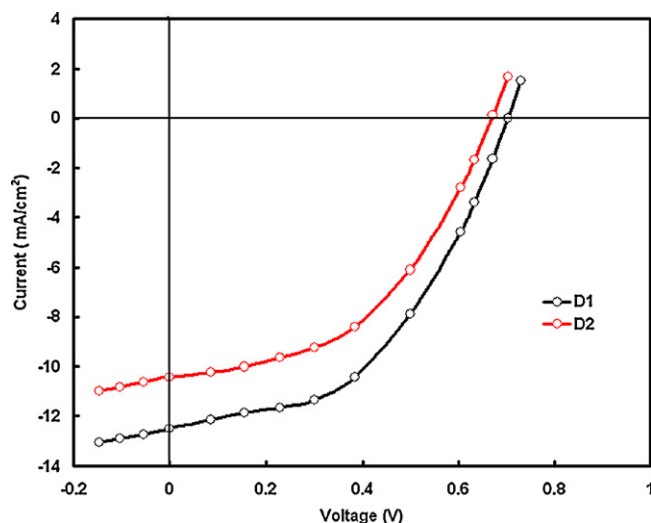
Fig. 7. Influence of co-adsorption of citric acid on the current–voltage characteristics of DSSCs based on **D1** and **D2** under illumination.

injected electrons within the TiO$_2$ porous films and the charge transfer process of the injected electrons at the interface between TiO$_2$ and electrolyte/dye coating. The high frequency peak (in the KHz range) is ascribed to the charge transport process at the interface between the redox couple and the platinum counter electrode. Fig. 8 shows the Bode phase plots of EIS spectra of the DSSCs made with TiO$_2$ electrodes dipped in dyes **D1** and **D2** with and without citric acid coadsorbent. The identical frequency peaks for both with and without coadsorbent in high frequency region indicates
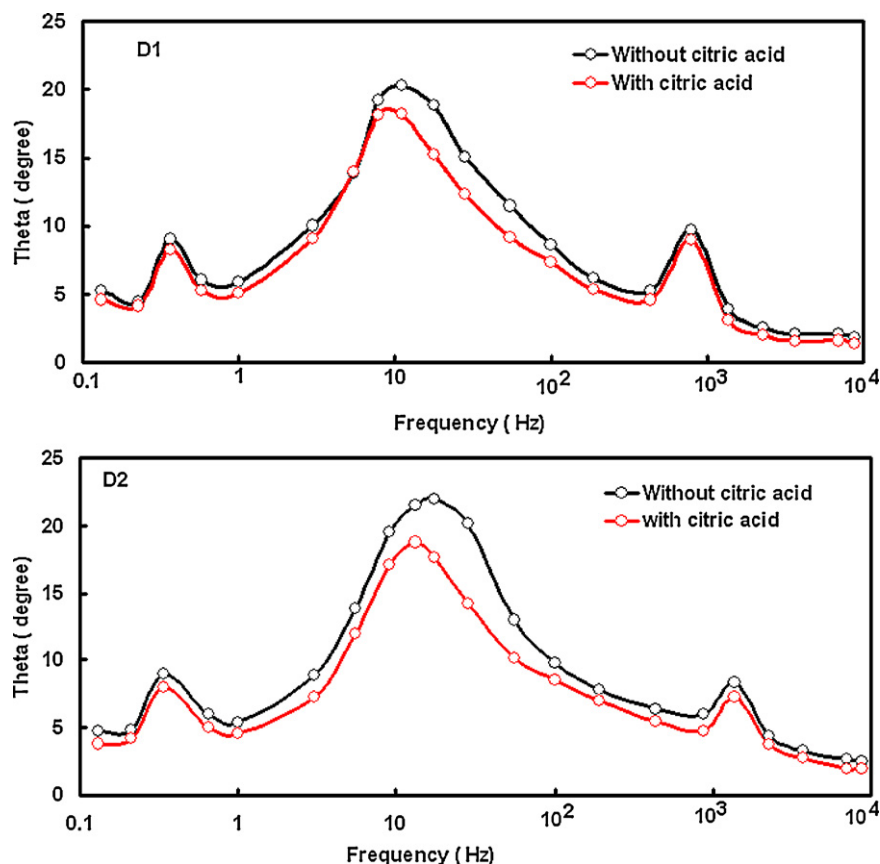
Fig. 8. Electrochemical impedance spectra (Bode plots) for DSSCs sensitized by **D1** and **D2** dyes with and without citric acid.

that the coadsorbent does not have any impact of the charge transfer at the Pt counter electrode/electrolyte interface. However, the middle frequency peak shifts to a smaller value with the addition of coadsorbent, indicating that the coadsorbent added to the dye solution influences the charge transfer process of the injected electrons from excited state of dye to conduction band of the TiO_2 film. According to EIS model developed by Kern et al. [40], the life time of the injected electrons in the TiO_2 film can be estimated from the position of the frequency peak (1–100 Hz range) in the Bode phase plots (Fig. 8) using the expression $\tau_n = (1/2\pi)f_c$, where f_c is the peak frequency of superimposed ac signal. The electron life time values derived from the Bode phase plots (Fig. 8) of EIS data are 14.4 ms and 22 ms for the DSSCs based on **D1** dye with and without coadsorbent, respectively. However, the values electron life time for the DSSCs based on **D2** dye with and without coadsorbent are 8 ms and 13 ms, respectively. The longer electron lifetime observed for **D1** as compared to **D2** indicated more effective suppression of back reaction of the injected electron with I_3^- in the electrolyte (recombination) and is also attributed to the improvements observed in the photocurrent and PCE. The further increase in the electron lifetime of injected electrons upon the addition of citric acid as a coadsorbent in the dye solution also indicates the back reaction of injected electron with the I_3^- in the electrolyte has been further reduced, resulting an increase in PCE of the DSSCs.

4. Conclusions

Three new bisazopyrroles and the corresponding BF_2-complexes were synthesised and used for DSSCs. Clear evidence for the complexation reaction was obtained from the FT-IR spectra of the dyes which showed new intense absorption around $1070 \, cm^{-1}$, as compared to the parent bisazopyrroles. Moreover, the complexation reaction of bisazopyrroles broadened and red shifted their absorption bands. The E_g^{opt} of the dyes was 1.49–1.70 eV. We have fabricated quasi solid state DSSCs using these dyes as sensitizers and found that the dye having COOH anchoring group shows higher PCE than other dyes having OH anchoring. This has been explained in the terms of longer electron lifetime of the injected electrons in TiO_2 film, which enhance both J_{sc} and V_{oc}. The co-adsorption of citric acid hindered the formation of dye aggregates and might improve the electron injection yield and thus J_{sc}. The enhancement in the V_{oc} is attributed to the decrease of charge recombination, confirmed by the increase in electron life time. The overall PCE for the DSSCs based on pyrrole dye with COOH groups containing the citric acid as coadsorbent is about 5.9%.

References

[1] Y. Ooyama, Y. Harima, Eur. J. Org. Chem. 18 (2009) 2903–2934.
[2] B. O'Regan, M. Grätzel, Nature 353 (1991) 737–740.
[3] H.A.M. van Mullekom, J.A.J.M. Vekemans, E.E. Havinga, E.W. Meijer, Mater. Sci. Eng. R 32 (2001) 1–40.
[4] (a) Y.J. Xia, X.Y. Deng, L. Wang, X.Z. Li, X.H. Zhu, Y. Cao, Macromol. Rapid Commun. 27 (2006) 1260–1264;
(b) D. Muehlbacher, M. Scharber, M. Morana, Z.G. Zhu, D. Waller, R. Gaudiana, C. Brabec, Adv. Mater. 18 (2006) 2884–2889;
(c) L.J. Hou, C. He, M.F. Han, E.J. Zhou, Y.F. Li, J. Polym. Sci. Part A: Polym. Chem. 45 (2007) 3861–3871;
(d) N. Blouin, A. Michaud, M. Leclerc, Adv. Mater. 19 (2007) 2295;
(e) Z.G. Zhu, D. Waller, R. Gaudiana, M. Morana, D. Muehlbacher, M. Scharber, C. Brabec, Macromolecules 40 (2007) 1981–1986;
(f) L. Liao, L.M. Dai, A. Smith, M. Durstock, J.P. Lu, J.F. Ding, Y. Tao, Macromolecules 40 (2007) 9406–9412.
[5] (a) R.Q. Yang, R.Y. Tian, J.G. Yan, Y. Zhang, J. Yang, Q. Hou, W. Yang, C. Zhang, Y. Cao, Macromolecules 38 (2005) 244–253;
(b) N. Blouin, A. Michaud, D. Gendron, S. Walkim, E. Blair, R. Neagu-Plesu, M. Belletete, G. Durocher, Y. Tao, M. Leclerc, J. Am. Chem. Soc. 130 (2008) 732–742.
[6] X.W. Zhan, Z.A. Tan, B. Domercq, Z.S. An, X. Zhang, S. Barlow, Y.F. Li, D.B. Zhu, B. Kippelen, S.R. Marder, J. Am. Chem. Soc. 129 (2007) 7246–7247.

[7] (a) B.C. Thompson, Y.G. Kim, T.D. McCarley, J.R. Reynolds, J. Am. Chem. Soc. 128 (2006) 12714–12725;
(b) K. Colladet, S. Fourier, T.J. Cleij, L. Lutsen, J. Gelan, D. Vanderzande, L.H. Nguyen, H. Neugebauer, S. Sariciftci, A. Aguirre, G. Janssen, E. Goovaerts, Macromolecules 40 (2007) 65–72.
[8] M.M. Wienk, M. Turbiez, J. Gilot, R.A.J. Janssen, Adv. Mater. 20 (2008) 2556–2560.
[9] E. Zhou, S. Yamakawa, K. Tajima, C. Yang, K. Hashimoto, Chem. Mater. 21 (2009) 4055–4061.
[10] L. Huo, J. Hou, H.-Y. Chen, S. Zhang, Y. Jiang, T.L. Chen, Y. Yang, Macromolecules 42 (2009) 6564–6571.
[11] E. Zhou, M. Nakamura, T. Nishizawa, Y. Zhang, Q. Wei, K. Tajima, C. Yang, K. Hashimoto, Macromolecules 41 (2008) 8302–8305.
[12] W. Yue, Y. Zhao, S. Shao, H. Tian, Z. Xie, Y. Geng, F. Wanga, J. Mater. Chem. 19 (2009) 2199–2206.
[13] M.S. Ho, C. Barrett, J. Paterson, M. Esteghamatian, A. Natansohn, P. Rochon, Macromolecules 29 (1996) 4613–4618.
[14] J.O.F. Boogers, P.T.A. Klaase, J.J. De Vlieger, D.P.W. Alkema, A.H.A. Tinnemans, Macromolecules 27 (1994) 197–204.
[15] S. Yin, H. Xu, W. Shi, Y. Gao, Y. Song, J.W.Y. Lam, B.Z. Tang, Polymer 46 (2005) 7670–7677.
[16] M.S. Ho, A. Natansohn, Macromolecules 28 (1995) 6124–6127.
[17] Y. Nabeshima, A. Shishido, A. Kanazawa, T. Shiono, T. Ikeda, T. Hiyama, Chem. Mater. 9 (1997) 1480–1487.
[18] A. Vig, K. Sirbiladze, H.J. Nagy, P. Aranyosi, I. Rusznák, P. Sallay, Dyes Pigments 71 (2006) 199–205.
[19] M.M.M. Raposo, A.M.R.C. Sousa, A.M.C. Fonseca, G. Kirsch, Tetrahedron 61 (2005) 8249–8256.
[20] K. Higashino, T. Nakayab, E. Ishiguro, J. Photochem. Photobiol. A: Chem. 79 (1994) 81–88.
[21] Y. Li, Brian, O. Patrick, D. Dolphin, J. Org. Chem. 74 (2009) 5237–5243.
[22] Y.S. Yen, Y.C. Hsu, J.T. Lin, C.W. Chang, C.P. Hsu, D. Yin, J. Phys. Chem. C 112 (2008) 12557–12567.
[23] P.M. Sommeling, B.C. O'Regan, R.R. Haswell, H.J.P. Smit, N.J. Bakker, J.J.T. Smits, J.M. Kroon, J.A.M. van oosmalen, J. Phys. Chem. B 110 (2006) 19191–19197.
[24] S. Ito, P. Liska, P. Comte, R. Charvet, P. Pechy, U. Bach, L. Schmidt-Menade, S.M. Zakeeruddin, A. Kay, M.K. Nazeeruddin, et al., Chem. Commun. 34 (2005) 4351–4353.
[25] J.A. Mikroyannidis, G.D. Sharma, S.S. Sharma, Y.K. Vijay, J. Phys. Chem. C 114 (2010) 1520–1527.
[26] S. Qu, W. Wu, J. Hua, C. Kong, Y. Long, H. Tian, J. Phys. Chem. C 114 (2010) 1343–1349.
[27] K. Hara, Z.S. Wang, T. Sato, A. Furube, R. Katoh, H. Sugihara, Y. Dan-oh, C. Kasada, A. Shinpo, S. Suga, J. Phys. Chem. B 109 (2005) 15476–15482.
[28] A. Hagfeldt, M. Grätzel, Chem. Rev. 95 (1995) 49–68.
[29] (a) S. Ito, S.M. Zakeeruddin, R. Humphry-Baker, P. Liska, R. Charvet, P. Comte, M.K. Nazeeruddin, P. Pechy, M. Takata, H. Miura, S. Uchida, M. Grätzel, Adv. Mater. 18 (2006) 1202–1205;
(b) Z.J. Ning, Q. Zhang, W.J. Wu, H.C. Pei, B. Liu, H. Tian, J. Org. Chem. 73 (2008) 3791–3797;
(c) R.Z. Li, D. Shi, D.F. Zhou, Y.M. Cheng, G.L. Zhnag, P. Wang, J. Phys. Chem. C 113 (2009) 7469–7479.
[30] M. Miyashita, K. Sunahara, T. Nishikawa, Y. Uemura, N. Koumura, K. Hara, A. Mori, T. Abe, E. Suzuki, S. Mori, J. Am. Chem. Soc. 130 (2008) 17874–17881.
[31] (a) S. Tatay, S.A. Haque, B. O'Regan, J.R. Durrant, W.J.H. Verhees, J.M. Kroon, A. Vidal-Ferran, P. Gavina, E. Palomares, J. Mater. Chem. 17 (2007) 3037–3044;
(b) K. Sayama, S. Tsukagoshi, K. Hara, Y. Ohga, A. Shinpou, Y. Abe, S. Suga, H. Arakawa, J. Phys. Chem. B 106 (2002) 1363–1371;
(c) H. Tian, X. Yang, R. Chen, R. Zhang, A. Hagfeldt, L. Sun, J. Phys. Chem. C 112 (2008) 11023–11033.
[32] (a) G. Boschloo, L. Haeggman, A. Hagfeldt, J. Phys. Chem. B 110 (2006) 13144–13150;
(b) M. Ikeda, N. Koida, L. Han, A. Sasahara, H. Onishi, Langmuir 24 (2008) 8056–8060.
[33] Z.S. Wang, Y. Cui, Y. Dan-oh, C. Kasada, A. Shinpo, K. Hara, J. Phys. Chem. C 111 (2007) 7224–7230.
[34] P. Wang, S.M. Zakeeruddin, P. Compte, R. Charvet, R. Humphry-Bakar, M. Grätzel, J. Phys. Chem. B 107 (2003) 14336–14341.
[35] N. Kopidakis, R. Neale Nathan, J. Frank Arthur, J. Phys. Chem. B 110 (2006) 12485–12489.
[36] M. Durr, A. Yasuda, G. Nelles, Appl. Phys. Lett. 89 (2006), 06110/1–06110/3.
[37] (a) E. Reynal, Palomares, Energy Environ. Sci. 2 (2009) 1078–1081;
(b) K.M. Lee, V. Suryanarayanan, K.C. Ho, T.K.R. Justin, J.T. Lin, Sol. Energy Mater. Sol. Cells 91 (2007) 1426–1431.
[38] (a) J. van de Lagemaat, N.G. Park, A.J. Frank, J. Phys. Chem. B 104 (2000) 2044–2052;
(b) Z. Zhang, S.M. Zakeeruddin, B.C. O'Regan, R. Humphry-Baker, M. Grätzel, J. Phys. Chem. B 109 (2005) 21818–21824.
[39] (a) S. Wang, Y. Li, C. Du, Z. Shi, S. Xiao, D. Zhua, E. Gao, S. Cai, Synth. Met. 128 (2002) 299–304;
(b) B.C. O'Regan, J.R. Durrant, P.M. Sommeling, N.J. Bakker, J. Phys. Chem. C 111 (2007) 14001–14010.
[40] R. Kern, R. Sastrawan, J. Ferber, R. Stangl, J. Luther, Electrochim. Acta 47 (2002) 4213–4225.